Inorg. Chem. **2006**, *45*, 8297–8307

Influence of Hartree–Fock Exchange on the Calculated Mössbauer Isomer Shifts and Quadrupole Splittings in Ferrocene Derivatives Using Density Functional Theory

Victor N. Nemykin* and Ryan G. Hadt

Department of Chemistry and Biochemistry, University of Minnesota Duluth, Duluth, Minnesota 55812

Received June 27, 2006

Influence of molecular geometry, type of exchange–correlation functional, and contraction scheme of basis set applied at the iron nuclei have been tested in the calculation of ^{57}Fe Mössbauer isomer shifts and quadrupole splittings for a wide range of ligand types, as well as oxidation and spin states, in inorganic and organometallic systems. It has been found that uncontraction of the s-part of Wachter's full-electron basis set at the iron nuclei does not appreciably improve the calculated isomer shifts. The observed correlations for all tested sets of geometries are close to each other and predominantly depend on the employed exchange–correlation functional with B3LYP functional being slightly better as compared to BPW91. Both hybrid (B3LYP) and pure (BPW91) exchange–correlation functionals are suitable for the calculation of isomer shifts in organometallic compounds. Surprisingly, it has been found that the hybrid B3LYP exchange–correlation functional completely fails in accurate prediction of quadrupole splittings in ferrocenes, while performance of the pure BPW91 functional for the same systems was excellent. This observation has been explained on the basis of relationship between the amount of Hartree–Fock exchange involved in the applied exchange–correlation functional and the calculated HOMO–LUMO energy gap in ferrocenes. On the basis of this explanation, use of only pure exchange–correlation functionals has been suggested for accurate prediction of Mössbauer spectra parameters in ferrocenes.

Introduction

Preparation of nanoscale materials with discrete properties is of great fundamental and technological interest.[1−5] Because of the current technological limitations (i.e., silicon-based technology), the majority of nanoelectronic devices require the presence of thermally stable molecules as key components, and numerous organometallic compounds were considered for application in nanomaterial constituents.[6,7] In particular, ferrocene and its derivatives are among interesting candidates because of their thermal stability and well-known simple synthetic transformation pathways.[8−10] In addition, polyferrocenes have some unique properties, i.e., mixed-valence state formation, and the chemistry of poly(metallocenes) with metal−metal coupling has resulted in a tremendous variety of remarkable structures interesting both from the fundamental nature of interaction between the metal centers (i.e., multiredox processes, magnetic coupling, and unpaired electron density migration) and practical points of view (i.e., optoelectronic materials for application in high-speed photonic or high-density memory devices).[11−14] We

* To whom correspondence should be addressed. E-mail: vnemykin@d.umn.edu.

(1) Hurst, S. J.; Payne, E. Kathryn; Qin, L.; Mirkin, C. A. *Angew. Chem., Int. Ed.* **2006**, *45*, 2672−2692.
(2) Wei, A. *Chem. Commun.* **2006**, 1581−1591.
(3) *Nanomaterials: New Research*; Caruta, B. M. Ed.; Nova Science Publishers: Hauppauge, New York, 2005; pp 239.
(4) *Comprehensive Coordination Chemistry II, Volume 7: From the Molecular to the Nanoscale: Synthesis, Structure, and Properties*; Fujita, M., Powell, A., Creutz, C., Eds.; Elsevier Ltd.: Oxford, UK, 2004; pp 845.
(5) *Nanomaterials: Synthesis, Properties and Application*; Edelstein, A. S., Cammarata, R. C., Eds.; Institute of Physics: Bristol, UK, 1996; pp 596.
(6) Braunstein, P. *J. Organomet. Chem.* **2004**, *689*, 3953−3967.
(7) Corriu, R.; Mehdi, A.; Reye, C. *J. Organomet. Chem.* **2004**, *689*, 4437−4450.
(8) Nishihara, H.; Kurihara, M. *Kagaku Kogyo* **2001**, *52*, 615−621.
(9) Elias A L.; Rodriguez-Manzo J A.; McCartney M R.; Golberg D.; Zamudio A.; Baltazar S E.; Lopez-Urias F.; Munoz-Sandoval E.; Gu L.; Tang C C.; Smith D J.; Bando Y.; Terrones H.; Terrones M. *Nano lett.* **2005**, *5*, 467−472.
(10) Li, Q.; Mathur, G.; Gowda, S.; Surthi, S.; Zhao, Q.; Yu, L.; Lindsey, J. S.; Bocian, D. F.; Misra, V. *Adv. Mater.* **2004**, *16*, 133−137.
(11) Miller, J. S.; Epstein, A. *Angew. Chem., Int. Ed. Engl.* **1994**, *33*, 385−415.
(12) Epstein, A. J.; Miller, J. S. *Synth. Met.* **1996**, *80*, 231−237.
(13) Barlow, S.; O'Hare, D. *Chem. Rev.* **1997**, *97*, 637−669.

10.1021/ic061176q CCC: $33.50
Published on Web 08/22/2006

are interested in the theoretical prediction of spectroscopic properties in ferrocene-containing compounds prepared and tested by our group as potential candidates for molecular electronics devices.

Among numerous spectroscopic methods useful for characterization of organometallic compounds, ^{57}Fe Mössbauer spectroscopy proved to be one of the most powerful techniques in determining valence and spin states, as well as detailed electronic structure, in numerous iron-containing inorganic and organometallic compounds.[15−17] In particular, ^{57}Fe Mössbauer spectroscopy has been successfully applied in investigation of the formation, stability, dynamics, and electron delocalization in mixed-valence polyferrocenes.[18−22] Moreover, it is probably the most convenient method for differentiating between mixed-valence classes in iron-containing mixed-valence complexes.[23−26]

Modern density functional theory (DFT) methods have been successfully applied recently for the calculation of Mössbauer isomer shifts and quadrupole splittings in numerous iron-containing compounds, including small inorganic molecules,[27−31] porphyrins,[32−35] phthalocyanines,[36] and bioinorganic-related compounds.[37−41] On the other hand, the theoretical modeling of Mössbauer spectral parameters in iron-containing organometallic complexes has been a long-time challenge until recently, when isomer shifts and quadrupole splittings for several half-sandwich and butadiene-containing iron compounds were tested by Oldfield's group using a DFT approach,[42−44] while the nature of quadrupole splitting in ferrocene has been discussed by Schwerdtfeger et al.[45] To the best of our knowledge, however, a systematic study on the modeling of Mössbauer spectra parameters in ferrocenyl-containing compounds has never been targeted.

In the present paper, we have systematically investigated an influence of exchange−correlation functional, basis set, and geometry on calculated isomer shifts and quadrupole splittings in numerous inorganic and organometallic compounds in an attempt to establish a reasonable approach for the prediction of Mössbauer spectra parameters in organometallic ferrocene-type complexes.

Computational Details

All DFT calculations were conducted using the Gaussian 03 software package[46] running under either Windows or UNIX OS. The spin-unrestricted method has been used for all paramagnetic complexes under consideration. In the present investigation, we have tested three sets of molecular geometries. The first set consists of X-ray-determined geometries available at Cambridge Structural Database[47] (abbreviations: Fc, ferrocene; $[Fc]^+$, ferricinium; Cp, cyclopentadiene; FcCN, cyanoferrocene; FcCOMe, acetylferrocene; $Fc(COMe)_2$, 1,1′-diacetylferrocene; FcC≡CH, ethynylferrocene; $Fc(CO_2Me)$, methyl ferrocenecarboxylate; $Fc(CO_2Me)_2$, 1,1′-methyl ferrocenedicarboxylate; $Fc(CO_2H)$, ferrocene carboxylic acid; $Fc(CO_2H)_2$, ferrocene 1,1′-dicarboxylic acid; $FcCN_3Vy$, 1,1,2-tricyanovinylferrocene; bipy, 2,2′-bipyridyne; phen, 1,10-phenantroline;

(14) Barlow, S. *Inorg. Chem.* **2001**, *40*, 7047−7053.
(15) Clark, S. J.; Donaldson, J. D.; Grimes, S. M. *Spectrosc. Prop. Inorg. Organomet. Comput.* **1997**, *30*, 380−453.
(16) *Mössbauer Spectroscopy of Frozen Solutions;* Vertes, A., Nagy, D. L. Eds.; 1990; pp 303.
(17) Reiff, W. M. *Mol. Cryst. Liq. Cryst.* **1989**, *176*, 391−414.
(18) Mochida, T.; Takazawa, K.; Matsui, H.; Takahashi, M.; Takeda, M.; Sato, M.; Nishio, Y.; Kajita, K.; Mori, H. *Inorg. Chem.* **2005**, *44*, 8628−8641.
(19) Pannell, K. H.; Imshennik, V. I.; Maksimov, Yu. V.; Il'ina, M. N.; Sharma, H. K.; Papkov, V. S.; Suzdalev, I. P. *Chem. Mater.* **2005**, *17*, 1844−1850.
(20) Oda, T.; Nakashima, S.; Okuda, T. *Inorg. Chem.* **2003**, *42*, 5376−5383.
(21) Jiao, J.; Long, G. J.; Grandjean, F.; Beatty, A. M.; Fehlner, T. P. *J. Am. Chem. Soc.* **2003**, *125*, 7522−7523.
(22) Nakashima, S.; Ueki, Y.; Sakai, H.; Maeda, Y. *J. Chem. Soc., Dalton Trans.* **1996**, 139−143.
(23) Kramer, J. A.; Herbstein, F. H.; Hendrickson, D. N. *J. Am. Chem. Soc.* **1980**, *102*, 2293−2301.
(24) Geiss, A.; Kolm, M. J.; Janiak, C.; Vahrenkamp, H. *Inorg. Chem.* **2000**, *39*, 4037−4043.
(25) Desbois, M. H.; Astruc, D.; Guillin, J.; Varret, F. *Organometallics* **1989**, *8*, 1848−1851.
(26) Drueeke, S.; Chaudhuri, P.; Pohl, K.; Wieghardt, K.; Ding, X. Q.; Bill, E.; Sawaryn, A.; Trautwein, A. X.; Winkler, H.; Gurman, S. *J. Chem. Soc., Chem. Commun.* **1989**, 59−62.
(27) Chanda, A.; Popescu, D.-L.; Tiago de Oliveira, F.; Bominaar, E. L.; Ryabov, A. D.; Münck, E.; Collins, T. *J. Inorg. Biochem.* **2006**, *100*, 606−619.
(28) Liu, T.; Lovell, T.; Han, W.-G.; Noodleman, L. *Inorg. Chem.* **2003**, *42*, 5244−5251.
(29) Zhang, Y.; Oldfield, E. *J. Phys. Chem. B* **2003**, *107*, 7180−7188.
(30) Han, W.-G.; Lovell, T.; Liu, T.; Noodleman, L. *Inorg. Chem.* **2003**, *42*, 2751−2758.
(31) Li, M.; Bonnet, D.; Bill, E.; Neese, F.; Weyhermueller, T.; Blum, N.; Sellmann, D.; Wieghardt, K. *Inorg. Chem.* **2002**, *41*, 3444−3456.
(32) Schoeneboom, J. C.; Neese, F.; Thiel, W. *J. Am. Chem. Soc.* **2005**, *127*, 5840−5853.
(33) Sinnecker, S.; Slep, L. D.; Bill, E.; Neese, F. *Inorg. Chem.* **2005**, *44*, 2245−2254.
(34) Smith, D. M. A.; Dupuis, M.; Straatsma, T. P. *Mol. Phys.* **2005**, *103*, 273−278.
(35) Zhang, Y.; Gossman, W.; Oldfield, E. *J. Am. Chem. Soc.* **2003**, *125*, 16387−16396.
(36) Nemykin, V. N.; Kobayashi, N.; Chernii, V. Y.; Belsky, V. K. *Eur. J. Inorg. Chem.* **2001**, 733−743.
(37) Han, W.-G.; Liu, T.; Lovell, T.; Noodleman, L. *J. Inorg. Biochem.* **2006**, *100*, 771−779.
(38) Horner, O.; Oddou, J.-L.; Mouesca, J.-M.; Jouve, H. M. *J. Inorg. Biochem.* **2006**, *100*, 477−479.
(39) Han, W.-G.; Liu, T.; Lovell, T.; Noodleman, L. *J. Am. Chem. Soc.* **2005**, *127*, 15778−15790.
(40) Krebs, C.; Price, J. C.; Baldwin, J.; Saleh, L.; Green, M. T.; Bollinger, J. Martin, Jr. *Inorg. Chem.* **2005**, *44*, 742−757.
(41) Zhang, Y.; Oldfield, E. *J. Am. Chem. Soc.* **2004**, *126*, 4470−4471.
(42) Havlin, R. H.; Godbout, N.; Salzmann, R.; Wojdelski, M.; Arnold, W.; Schulz, C. E.; Oldfield, E. *J. Am. Chem. Soc.* **1998**, *120*, 3144−3151.
(43) Zhang, Y.; Mao, J.; Godbout, N.; Oldfield, E. *J. Am. Chem. Soc.* **2002**, *124*, 13921−13930.
(44) Zhang, Y.; Mao, J.; Oldfield, E. *J. Am. Chem. Soc.* **2002**, *124*, 7829−7839.
(45) Schwerdtfeger, P.; Sohnel, T.; Pernpointner, M.; Laerdahl, J. K.; Wagner, F. E. *J. Chem. Phys.* **2001**, *115*, 5913−5924.
(46) Frisch, M. J.; Trucks, G. W.; Schlegel, H. B.; Scuseria, G. E.; Robb, M. A.; Cheeseman, J. R.; Montgomery, J. A., Jr.; Vreven, T.; Kudin, K. N.; Burant, J. C.; Millam, J. M.; Iyengar, S. S.; Tomasi, J.; Barone, V.; Mennucci, B.; Cossi, M.; Scalmani, G.; Rega, N.; Petersson, G. A.; Nakatsuji, H.; Hada, M.; Ehara, M.; Toyota, K.; Fukuda, R.; Hasegawa, J.; Ishida, M.; Nakajima, T.; Honda, Y.; Kitao, O.; Nakai, H.; Klene, M.; Li, X.; Knox, J. E.; Hratchian, H. P.; Cross, J. B.; Bakken, V.; Adamo, C.; Jaramillo, J.; Gomperts, R.; Stratmann, R. E.; Yazyev, O.; Austin, A. J.; Cammi, R.; Pomelli, C.; Ochterski, J. W.; Ayala, P. Y.; Morokuma, K.; Voth, G. A.; Salvador, P.; Dannenberg, J. J.; Zakrzewski, V. G.; Dapprich, S.; Daniels, A. D.; Strain, M. C.; Farkas, O.; Malick, D. K.; Rabuck, A. D.; Raghavachari, K.; Foresman, J. B.; Ortiz, J. V.; Cui, Q.; Baboul, A. G.; Clifford, S.; Cioslowski, J.; Stefanov, B. B.; Liu, G.; Liashenko, A.; Piskorz, P.; Komaromi, I.; Martin, R. L.; Fox, D. J.; Keith, T.; Al-Laham, M. A.; Peng, C. Y.; Nanayakkara, A.; Challacombe, M.; Gill, P. M. W.; Johnson, B.; Chen, W.; Wong, M. W.; Gonzalez, C.; Pople, J. A. *Gaussian 03*, revision C.02; Gaussian, Inc.: Wallingford, CT, 2004.
(47) CCDC database, V5.27, Cambridge, U.K.; Nov 2005.

Table 1. Comparison of X-ray Determined and B3LYP and BP86 Optimized Bond Distances in Some Organometallic Compounds

	X-ray		B3LYP		BP86	
compound	Fe−C	Fe−L	Fe−C	Fe−L	Fe−C	Fe−L
(butadiene)$Fe(CO)_3$	2.100	1.763 (CO)	2.108	1.802 (CO)	2.104	1.788 (CO)
(cyclobutadiene) $Fe(CO)_3$	2.048	1.763 (CO)	2.060	1.798 (CO)	2.053	1.786 (CO)
$CpFe(CO)_2Cl$	2.070	1.771 (CO)	2.143	1.802 (CO)	2.124	1.769 (CO)
		2.288 (Cl)		2.310 (Cl)		2.306 (Cl)
$CpFe(CO)_2Me$	2.075	1.771 (CO)	2.150	1.771 (CO)	2.132	1.752 (CO)
		1.930 (Me)		2.054 (Me)		2.060 (Me)
Fc D_{5d}	2.012		2.082		2.009	
Fc D_{5h}	2.060		2.078		2.055	
FcCN	2.037		2.078		2.055	
$FcVyCN_3$	2.085		2.082		2.082	

Pc, phthalocyanine; mepip, 4-methylpiperidine). In the second set, the structures were optimized at Becke's three-parameter hybrid exchange functional[48] and Lee−Yang−Parr nonlocal correlation functional[49] (B3LYP) level coupled with Wachter's full-electron basis set for the iron atom and 6-31G(d)[50] basis set for all other atoms geometries. The third set of geometries was obtained via optimization at Becke's exchange functional[51] and Perdew's nonlocal correlation functional[52] (BP86) level coupled with the same basis set combination as mentioned above. For all optimized structures, frequency calculations were carried out to ensure optimized geometries represented local minima. For all organometallic compounds tested in this work, a very good agreement between X-ray-determined and optimized structures for all metal-to-ligand distances has been observed (Table 1).

In the case of single-point calculations, for all compounds, hybrid B3LYP and Becke's pure exchange−functional and Perdew and Wang's correlation functional[53] (BPW91) were tested. Wachter's original full-electron basis set[54] (contracted as 62111111/3311111/3111) with one set of polarization functions was used for the iron atom, while for all other atoms the 6-311G(d) basis set was employed (this combination of the basis sets is designated as Wf below). In the other set of single-point calculations, the s-part of Wachter's full-electron basis set employed at the iron atom was completely uncontracted, while the 6-311G(d)[55] basis set was applied for all other atoms (this combination of the basis sets is designated as WfsU below). In the case of Wf basis set combination, the ultra fine integral grid with 99 radial shells and 590 angular points per shell has been used, while for the WfsU basis set combination, an integral grid with 250 radial shells and 770 angular points per shell has been utilized because the above-mentioned modification of basis set requires a more precise integration grid. In all cases, the tight energy (10^{-8} au) SCF convergence criterion has been used.

Electron densities on the ^{57}Fe nuclei in the compounds of interest were calculated using the AIM2000[56] program, which utilizes wave functions generated by Gaussian software. Mössbauer quadrupole splittings (ΔE_Q) and asymmetry parameters (η) were calculated using DFT predicted principal components of the electric field gradient tensor (V_{ii}) at the ^{57}Fe nucleus as discussed below.

Results and Discussion

Isomer Shifts. The isomer shift in Mössbauer spectra arises from differences in electron density at the nucleus in the absorber and a reference compound (typically α-Fe or sodium nitroprusside). It can be calculated using the following equation:[57,58]

$$\delta_{\alpha Fe} = E_A - E_{\alpha Fe} = (2\pi/3)Ze^2([R^2]^* - [R^2])(|\Psi(0)|_A^2 - |\Psi(0)|_{\alpha Fe}^2) \quad (1)$$

where Z is the atomic number of the nuclei of interest and R and R^* are the average nuclear radii of the ground and excited states of ^{57}Fe, respectively. Due to the fact that $|\Psi(0)|_{\alpha Fe}^2$ is the constant, the Mössbauer isomer shift can be calculated as[57,58]

$$\delta_{\alpha Fe} = \alpha[\rho(0) - c] \quad (2)$$

where α is the so-called calibration constant and $\rho(0)$ is the nonrelativistic calculated total charge density at the iron nucleus. The calibration constant, α, and parameter, c, can be easily obtained from a correlation analysis between calculated $\rho(0)$ and experimentally observed $\delta_{\alpha Fe}$. As has been mentioned previously,[33,59] the calculated $\rho(0)$ depends on the applied exchange−correlation functional, as well as basis set, and thus, every combination of exchange−correlation functional and basis set should be calibrated separately. Thus far, the most of predicted Mössbauer isomer shifts were calculated using B3LYP, BPW91, and BP86 exchange−correlation functionals,[28,29,31,32] and below we will compare the results obtained from hybrid B3LYP and pure BPW91 approaches. Another question which will be addressed below belongs to the flexibility of basis set applied on the iron atom. In particular, we would like to test a current controversy about the necessity in increasing flexibility of the s-part of the basis set for correct calculation of Mössbauer isomer shifts. For instance, Oldfield's,[35,42,43] Noodleman's,[28,30] and our group[36] have successfully used GTO or STO basis sets contracted in the core s-electron region. On the other hand, Neese[59] proposed the use of a completely s-part

(48) Becke, A. D. *Phys. Rev. A* **1988**, *38*, 3098−3100.
(49) Lee, C.; Yang, W.; Parr, R. G. *Phys. Rev. B* **1988**, *37*, 785−789.
(50) McLean McLean, A. D.; Chandler, G. S. *J. Chem. Phys.* **1980**, *72*, 5639−5948.
(51) Becke, A. D. *Phys. Rev. A* **1988**, *38*, 3098−3100.
(52) Lee, C.; Yang, W.; Parr, R. G. *Phys. Rev. B* **1988**, *37*, 785−789.
(53) Perdew, J. P.; Wang, Y. *Phys. Rev. B* **1992**, *45*, 13244−13249.
(54) Wachters, A. J. H. *J. Chem. Phys.* **1970**, *52*, 1033−1036.
(55) Krishnan, R.; Binkley, J. S.; Seeger, R.; Pople, J. A. *J. Chem. Phys.* **1980**, *72*, 650−654.
(56) (a) Biegler-Konig, F. *AIM2000*, version 1.0; University of Applied Science: Bielefeld, Germany. (b) Bader, R. F. W. *Atoms in Molecules A Quantum Theory*; Oxford University Press: Oxford, 1990.
(57) Fluck, E. In *Chemical Applications of Mössbauer Spectroscopy*; Goldanskii, V. I., Herber, R. H., Eds.; Academic Press, Inc.: New York 1968; pp 268−311.
(58) Gütlich P.; Ensling, J. In *Inorganic Electronic Structure and Spectroscopy*; Lever, A. B. P., Solomon, E. I., Eds.; John Wiley and Sons: New York 1999; Vol. I, pp 161−212.
(59) Neese, F. *Inorg. Chim. Acta* **2002**, *337*, 181−192.

uncontracted triple-ζ-quality basis set with several additional tight s-functions added to it. Such a complete uncontraction of the s-part of the basis set adds more flexibility in description of electron density close to the iron atom, and thus, at least theoretically, should result in more accurate calculation of isomer shifts in iron-containing compounds. The proposed advantage, however, comes with a significant increase in computational time due to necessary increase in quality of numerical integration for tightly contracted basis functions.[59] To address the above question, we used both contracted and s-part uncontracted basis sets at the iron atom with results discussed below. Next, as it has been recently pointed out by Neese's group,[33] the performance of nonrelativistic and quasi-relativistic DFT approaches is similar, and thus, only the computationally less expensive nonrelativistic method has been used in this paper. Finally, in most cases, both X-ray and optimized geometries were used[39,42,59] in the same test set of molecules, and we would like to clarify an influence of different geometries (i.e., optimized at different levels of theory and X-ray determined) on calculated Mössbauer spectra parameters. All three test sets of molecules include small inorganic and organometallic compounds along with the classic test set of complexes ($[FeF_6]$,$^{4-}$ $[FeF_6]^{3-}$, $[Fe(CN)_6]$,$^{4-}$ $[Fe(CN)_6]^{3-}$, and $[FeO_4]^{2-}$). Due to complexity of the Jahn−Teller energy surface (which will be discussed elsewhere), which results in difficulties with optimization of the correct ground state for $[FeF_6]^{4-}$ complex, this compound will not be discussed with the optimized geometry test sets.

First, an excellent correlation in the form of

$$\rho(0) = (1/\alpha)\,\delta_{\alpha Fe} + c \qquad (3)$$

between calculated total electron densities on the iron atom and experimental isomer shifts[60] has been observed for all three training set geometries (X-ray determined, BP86 optimized, and B3LYP optimized) coupled with BPW91 and B3LYP exchange−correlation functionals and both basis sets tested (Tables 2−4, Figure 1 and Supporting Information Figures 1 and 2). For all cases, correlation coefficients between 0.965 and 0.987 have been observed, suggesting, in the first approximation, that choice of starting geometry, exchange−correlation functional, and contraction scheme for Wachter's full-electron basis set is not critical for calculation of total electron densities at Mössbauer nuclei.

A closer look into the correlation coefficients and standard deviations supports an earlier observation[42,43] that the hybrid B3LYP exchange−correlation functional performs slightly better as compared to the pure BPW91 exchange−correlation functional for each geometry set tested. Interestingly, uncontraction of the s-part of Wachter's basis set, which improves the description of electron density close to the iron nucleus, brings no appreciable improvement on calculated isomer shift values in the large range of tested isomer shifts (2.34 mm/s). Moreover, in the case of the X-ray geometry test set, contracted Wachter's basis set performs slightly better as compared to the uncontracted one, while performance of contracted and uncontracted basis sets for the BP86 optimized geometries test set is the same. Rearrangement of eq 3 into the form of eq 2 and using a 1.3 correction factor between nonrelativistic and relativistic electron densities[61−64] allowed us to calculate a calibration constant, α_{rel}, between −0.308 and −0.357 for BPW91 and −0.291 and −0.320 for B3LYP data sets, which is in good agreement with the recent DFT-based estimations[44] with a higher α_{rel} predicted for pure BPW91 and a lower α_{rel} for the hybrid B3LYP exchange correlation functionals. For all cases tested, the standard deviation between calculated and experimental isomer shifts was to be found between 0.075 and 0.135 mm/s for the 2.34 mm/s range (Tables 2−4, Figure 2 and Supporting Information Figures 3 and 4), which brings the average errors for predicted isomer shifts between 3.21% and 5.77%, and this result should be considered as an excellent agreement between theory and experiment taking into account the broad variety of experimental temperatures in the test set of molecules.[60] Isomer shifts in organometallic compounds, and in particular for all ferrocenes, can be predicted well using both hybrid (B3LYP) and pure (BPW91) exchange−correlation functionals. Overall, each three geometry sets, both exchange−correlation functionals, and all basis sets lead to an acceptable prediction of isomer shifts in iron-containing complexes, and it seems that the flexibility of the original Wachter's basis set is sufficient enough for accurate calculation of total electron density around the iron atom.

Although it has been suggested that it is necessary to use a completely uncontracted in the s-part basis set with additional tight s-functions (with the highest exponent about 5 000 000),[59] it can be argued that so far we were not able to find a single compound for which the calculated total electronic density was in a strong disagreement with the expected value, and thus, use of a contracted basis set scheme (which makes it possible to calculate total electron densities 1.5−2.5 times faster as compared to those calculated using a tighter integration grid and uncontracted basis set) is suggested.

Quadrupole Splittings. The quadrapole splitting arises from a nonspherical charge distribution in the $I^* = 3/2$ excited state in the presence of an electric field gradient at the ^{57}Fe nucleus. It is related to the components of the electric field

(60) For the ideal test set, all experimental isomer shifts should be measured at 4.2 K (the lowest affordable cryostat temperature in Mössbauer spectroscopy) because a priori the Mössbauer isomer shift is temperature dependent. In the absence of solid-state phase transitions in Mössbauer sample, the isomer shift should increase linearly when temperature decreases and is described by the Debye−Waller factor, $f = e^{-k^2\langle x^2\rangle}$, where $\langle x^2\rangle$ is the mean square amplitude of vibration of the Mössbauer nucleus. The average vibrational amplitude at the Mössbauer nuclei is, strickly speaking, individual and varies significantly (when variable-temperature data are available) for every iron-containing compound discussed in this paper. Taking this fact into consideration, we prefer not to do any 'average' isomer shift adjastments proposed by Noodleman et al. (*Inorg. Chem.* **2003**, *42*, 5244−5251) for higher-temperature data in Tables 2−4 because such adjastments lead to the same error amplitude as use of the higher-temperature data.

(61) Desclaux, J. P. *Comput. Phys. Commun.* **1975**, *9*, 31−45.
(62) Mann, J. B. *J. Chem. Phys.* **1969**, *51*, 841−842.
(63) Trautwein, A.; Harris, F. E.; Freeman, A. J.; Desclaux, J. P. *Phys. Rev. B* **1975**, *11*, 4101−4105.
(64) Yamada, Y.; Tominaga, T. *Radiochim. Acta* **1998**, *80*, 163−170.

Table 2. Experimental ^{57}Fe Mössbauer Isomer Shifts, Calculated Total Electron Densities, and Isomer Shifts for the X-ray Geometry Test Set

			experimental		calculated							
					BPW91/Wf		BPW91/WfsU		B3LYP/Wf		B3LYP/WfsU	
compound	OS	S	T (K)	IS (mm/s)	ρ	IS (mm/s)	ρ	IS(mm/s)	ρ	IS (mm/s)	ρ	IS (mm/s)
$Fe(CO)_5$	0	0	143	−0.18[a]	11 617.75	−0.21	11 576.33	−0.22	11 614.48	−0.15	11 569.56	−0.15
(butadiene)$Fe(CO)_3$	0	0	77	0.03[b]	11 617.58	−0.15	11 576.17	−0.15	11 614.34	−0.09	11 569.43	−0.10
$CpFe(CO)_2Cl$	2	0	4.2	0.27[c]	11 616.92	0.14	11 575.54	0.15	11 613.64	0.18	11 568.76	0.18
$CpFe(CO)_3^+$	2	0	78	0.05[b]	11 617.23	0.01	11 575.83	0.01	11 613.96	0.06	11 569.06	0.05
Fc D_{5h}	2	0	80	0.53[b]	11 615.87	0.60	11 574.80	0.49	11 612.79	0.52	11 567.75	0.60
Fc D_{5d}	2	0	80	0.53[b]	11 616.08	0.51	11 575.00	0.40	11 612.79	0.52	11 567.95	0.52
FcCN	2	0	80	0.52[b]	11 615.99	0.55	11 574.65	0.56	11 612.68	0.56	11 567.84	0.56
$FcCN_3Vy$	2	0	RT	0.42[d]	11 615.98	0.55	11 574.64	0.57	11 612.69	0.56	11 567.85	0.56
FcC≡CH	2	0	90	0.52[e]	11 616.17	0.47	11 574.82	0.49	11 612.88	0.48	11 567.75	0.48
Fc(COMe)	2	0	80	0.54[f]	11 615.96	0.56	11 574.68	0.57	11 612.67	0.57	11 567.83	0.57
$Fc(COMe)_2$	2	0	80	0.49[f]	11 615.98	0.56	11 574.66	0.57	11 612.68	0.56	11 567.84	0.56
$Fc(CO_2Me)$	2	0	80	0.53[f]	11 616.03	0.53	11 574.68	0.54	11 612.74	0.54	11 567.90	0.54
$Fc(CO_2Me)_2$	2	0	80	0.54[f]	11 616.00	0.55	11 574.66	0.56	11 612.70	0.55	11 567.86	0.55
$Fc(CO_2H)$	2	0	RT	0.44[f]	11 616.01	0.54	11 574.67	0.56	11 612.72	0.55	11 567.88	0.55
$Fc(CO_2H)_2$	2	0	80	0.48[f]	11 616.00	0.55	11 574.66	0.56	11 612.71	0.55	11 567.87	0.55
$PcFePy_2$	2	0	4.2	0.32[g]	11 616.51	0.32	11 575.14	0.34	11 613.11	0.39	11 568.24	0.40
$PcFe(mepip)_2$	2	0	RT	0.27[g]	11 616.44	0.35	11 575.07	0.37	11 613.04	0.42	11 568.18	0.42
$[Fe(CN)_5NO]^{2-}$	2	0	77	−0.19[h]	11 617.86	−0.27	11 576.43	−0.26	11 614.76	−0.26	11 569.82	−0.26
$[Fe(CN)_6]^{4-}$	2	0	143	−0.07[a]	11 617.46	−0.02	11 576.04	−0.02	11 614.16	0.09	11 569.24	0.08
$Fe(phen)_2Cl_2$	2	2	77	1.07[h]	11 615.17	0.91	11 573.88	0.92	11 611.57	1.00	11 566.81	0.99
$Fe(bipy)_2Cl_2$	2	2	78	1.11[h]	11 615.29	0.86	11 574.00	0.89	11 611.70	0.95	11 566.93	0.94
$FePy_4Cl_2$	2	2	4.2	1.10[h]	11 614.92	1.02	11 573.64	1.03	11 611.40	1.07	11 566.63	1.07
$[Fe(H_2O)_6]^{2+}$	2	2	200	1.34[i]	11 614.11	1.37	11 572.89	1.38	11 610.68	1.35	11 565.97	1.34
$[FeF_6]^{4-}$ ($KFeF_3$)	2	2	0	1.44[a]	11 613.98	1.44	11 572.76	1.44	11 610.51	1.42	11 565.81	1.41
$[FeCl_4]^{2-}$	2	2	4.2	1.00[j]	11 615.02	0.98	11 573.75	0.98	11 611.69	0.96	11 566.93	0.94
$[Fc]^+$	3	1/2	78	0.50[f]	11 616.18	0.47	11 574.83	0.48	11 612.91	0.47	11 568.06	0.47
PcFeCl	3	5/2	77	0.28[g]	11 616.62	0.27	11 575.25	0.28	11 613.54	0.22	11 568.64	0.23
$[Fe(bipy)_2Cl_2]^+$	3	5/2	RT	0.42[j]	11 615.98	0.55	11 574.65	0.56	11 612.91	0.47	11 568.08	0.46
$[Fe(phen)_2Cl_2]^+$	3	5/2	80	0.39[b]	11 615.96	0.57	11 574.63	0.57	11 612.89	0.48	11 568.05	0.47
$[FeCl_4]^-$	3	5/2	77	0.30[h]	11 616.26	0.43	11 574.93	0.44	11 613.23	0.35	11 568.39	0.33
$[FeBr_4]^-$	3	5/2	77	0.36[h]	11 616.16	0.48	11 574.84	0.47	11 613.15	0.38	11 568.31	0.37
$[FeCl_6]^{3-}$	3	5/2	78	0.53[j]	11 615.71	0.67	11 574.42	0.67	11 612.66	0.57	11 567.57	0.67
$[Fe(H_2O)_6]^{3+}$	3	5/2	78	0.50[k]	11 616.12	0.49	11 574.79	0.49	11 613.02	0.43	11 568.19	0.42
$[FeF_6]^{3-}$	3	5/2	0	0.69[a]	11 615.75	0.66	11 574.46	0.65	11 612.61	0.59	11 567.81	0.58
$[Fe(CN)_6]^{3-}$	3	1/2	143	−0.15[a]	11 617.79	−0.24	11 576.36	−0.23	11 614.58	−0.19	11 569.65	−0.19
$[FeO_4]^{2-}$	6	1	143	−0.90[a]	11 619.45	−0.97	11 577.98	−0.98	11 616.71	−1.03	11 571.70	−1.05
r						0.978		0.977		0.987		0.985
rms						0.098		0.100		0.075		0.082
α_{rel}						−0.338		−0.357		−0.304		−0.320
c					11 617.24		11 575.86		11 614.10		11 569.19	

[a] Reference 73, see comments on isomer shift of $Fe(CO)_5$ in ref 80. [b] Reference 57. [c] Reference 74. [d] This work, see Supporting Information for details. [e] Reference 76. [f] Reference 78. [g] Reference 77. [h] Reference 58. [i] Reference 16. [j] Reference 75. [k] Reference 79.

gradient as represented by eq 4:[57,58]

$$\Delta E_Q = (1/2)eQV_{zz}\{1 + (\eta^2/3)\}^{1/2} \quad (4)$$

where e is the electron charge and Q is the quadrapole moment of the ^{57}Fe $E = 14.4$ keV excited state. In our case, we used the recently determined value of $Q = 0.16$ (±5%) barn,[65] which has been commonly used for the calculation of Mössbauer quadrupole splittings in DFT calculations and close to the value of 0.158 barn reported recently by Neese's group[33] from the nonrelativistic DFT B3LYP training set. The asymmetry parameter (η) is given by[57,58]

$$\eta = (V_{xx} - V_{yy})/V_{zz} \quad (5)$$

where the principal components of the electric field are taken as[57,58]

$$|V_{zz}| \geq |V_{yy}| \geq |V_{xx}| \quad (6)$$

Calculated quadrupole splittings for all three training sets of molecules are presented in Tables 5−7, while relationship between calculated and experimentally observed quadrupole splittings are shown in Figure 3 and Supporting Information Figures 5 and 6. In all cases, excellent correlations have been observed between calculated and experimental quadrupole splittings with correlation coefficients between 0.983 and 0.998.

An uncontraction of the s-part of the basis set should not significantly affect both electric field gradient elements, V_{ii}, and asymmetry parameter, η, because both of these parameters mostly depend on the correct description of electron distribution within the d- and p-orbitals in the valence region subspace.[57,58] Indeed, calculated electric field gradients and asymmetry parameters are close to each other for Wf and WfsU basis sets applied for the same molecular geometries and the same exchange−correlation functionals (Tables 5−7).

For the X-ray geometries test set, both pure and hybrid exchange−correlation functionals are ∼10% off the ideal 1.0

(65) Dufek, P.; Blaha, P.; Schwarz, K. *Phys. Rev. Lett.* **1995**, *75*, 3545−3548.

Table 3. Experimental ^{57}Fe Mössbauer Isomer Shifts, Calculated Total Electron Densities, and Isomer Shifts for the B3LYP Geometry Test Set

			experimental		calculated							
					BPW91/Wf		BPW91/WfsU		B3LYP/Wf		B3LYP/WfsU	
structure	OS	S	T (K)	IS (mm/s)	ρ	IS (mm/s)	ρ	IS (mm/s)	ρ	IS (mm/s)	ρ	IS (mm/s)
$[Fe(CO)_4]^{2-}$	−2	0	RT	−0.18[a]	11 617.86	−0.31	11 576.45	−0.32	11 614.66	−0.28	11 569.74	−0.28
$Fe(CO)_5$	0	0	143	−0.18	11 617.59	−0.20	11 576.19	−0.21	11 614.31	−0.15	11 569.41	−0.15
(cyclobutadiene)$Fe(CO)_3$	0	0	78	0.02[b]	11 617.59	−0.20	11 575.90	−0.09	11 614.05	−0.05	11 569.16	−0.05
(butadiene)$Fe(CO)_3$	0	0	77	0.03	11 617.26	−0.07	11 575.86	−0.08	11 614.00	−0.03	11 569.11	−0.03
$CpFe(CO)_2Me$	2	0	78	0.08	11 617.09	0.00	11 575.70	−0.01	11 613.82	0.03	11 568.94	0.03
$CpFe(CO)_2Cl$	2	0	4.2	0.27[b]	11 616.70	0.16	11 575.33	0.14	11 613.41	0.19	11 568.55	0.19
Fc D_{5h}	2	0	80	0.53	11 615.69	0.56	11 574.38	0.54	11 612.40	0.57	11 567.59	0.56
Fc D_{5d}	2	0	80	0.53	11 615.70	0.55	11 574.38	0.54	11 612.40	0.57	11 567.58	0.57
FcCN	2	0	80	0.52	11 615.74	0.54	11 574.41	0.53	11 612.44	0.56	11 567.62	0.55
$FcCN_3Vy$	2	0	RT	0.42	11 615.75	0.53	11 574.42	0.52	11 612.45	0.56	11 567.62	0.55
$[Fe(CN)_5NO]^{2-}$	2	0	77	−0.19	11 617.77	−0.27	11 576.34	−0.28	11 614.67	−0.28	11 569.74	−0.28
$[Fe(CN)_6]^{4-}$	2	0	143	−0.07	11 616.53	0.21	11 575.17	0.22	11 613.18	0.28	11 568.32	0.28
$[Fe(H_2O)_6]^{2+}$	2	2	200	1.34	11 613.87	1.28	11 572.66	1.25	11 610.45	1.31	11 565.75	1.29
$[FeCl_4]^{2-}$	2	2	4.2	1.00	11 614.71	0.95	11 573.46	0.92	11 611.39	0.95	11 566.65	0.94
$[FeCl_4]^{-}$	3	5/2	77	0.30	11 616.08	0.40	11 574.76	0.38	11 613.07	0.32	11 568.24	0.31
$[FeBr_4]^{-}$	3	5/2	77	0.36	11 616.06	0.41	11 574.74	0.39	11 613.06	0.32	11 568.23	0.31
$[FeCl_6]^{3-}$	3	5/2	78	0.53	11 615.40	0.67	11 574.12	0.65	11 612.38	0.58	11 567.57	0.57
$[Fe(H_2O)_6]^{3+}$	3	5/2	78	0.50	11 615.36	0.69	11 574.08	0.66	11 612.38	0.58	11 567.59	0.57
$[FeF_6]^{3-}$	3	5/2	0	0.69	11 615.91	0.47	11 574.08	0.66	11 612.74	0.44	11 567.59	0.56
$[Fe(CN)_6]^{3-}$	3	1/2	143	−0.15	11 617.11	0.01	11 575.72	−0.02	11 613.91	0.00	11 569.01	0.00
$[FeO_4]^{2-}$	6	1	143	−0.90	11 619.38	−0.92	11 577.91	−0.93	11 616.63	−1.03	11 571.63	−1.03
r						0.965		0.975		0.969		0.974
rms						0.135		0.113		0.125		0.114
α_{rel}						−0.308		−0.320		−0.291		−0.308
c					11 617.08		11 575.68		11 613.91		11 569.02	

[a] Reference 74. [b] Reference 58.

Table 4. Experimental ^{57}Fe Mössbauer Isomer Shifts, Calculated Total Electron Densities, and Isomer Shifts for the BP86 Geometry Test Set

			experimental		calculated							
					BPW91/Wf		BPW91/WfsU		B3LYP/Wf		B3LYP/WfsU	
structure	OS	S	T (K)	IS (mm/s)	ρ	IS (mm/s)	ρ	IS (mm/s)	ρ	IS (mm/s)	ρ	IS (mm/s)
$[Fe(CO)_4]^{2-}$	−2	0	RT	−0.18	11 617.81	−0.27	11 576.40	−0.27	11 614.61	−0.23	11 569.70	−0.23
$Fe(CO)_5$	0	0	143	−0.18	11 617.73	−0.23	11 576.32	−0.23	11 614.46	−0.17	11 569.55	−0.17
(cyclobutadiene)$Fe(CO)_3$	0	0	78	0.02	11 617.39	−0.10	11 575.99	−0.10	11 614.15	−0.06	11 569.25	−0.05
(butadiene)$Fe(CO)_3$	0	0	77	0.03	11 617.38	−0.09	11 575.98	−0.09	11 614.13	−0.05	11 569.23	−0.04
$CpFe(CO)_2Me$	2	0	78	0.08	11 617.23	−0.03	11 575.84	−0.03	11 613.98	0.01	11 569.09	0.02
$CpFe(CO)_2Cl$	2	0	4.2	0.27	11 616.92	0.09	11 575.55	0.10	11 613.65	0.14	11 568.78	0.14
Fc D_{5h}	2	0	80	0.53	11 615.88	0.52	11 574.56	0.52	11 612.60	0.54	11 567.78	0.54
Fc D_{5d}	2	0	80	0.53	11 615.89	0.51	11 574.56	0.52	11 612.60	0.54	11 567.77	0.54
FcCN	2	0	80	0.52	11 615.92	0.50	11 574.59	0.51	11 612.64	0.52	11 567.80	0.53
$FcCN_3Vy$	2	0	RT	0.42	11 615.93	0.50	11 574.59	0.51	11 612.63	0.53	11 567.80	0.53
$[Fe(CN)_5NO]^{2-}$	2	0	77	−0.19	11 617.80	−0.26	11 576.37	−0.26	11 614.70	−0.26	11 569.77	−0.25
$[Fe(CN)_6]^{4-}$	2	0	143	−0.07	11 616.99	0.07	11 575.60	0.07	11 613.66	0.13	11 568.77	0.14
$[Fe(H_2O)_6]^{2+}$	2	2	200	1.34	11 613.96	1.30	11 572.74	1.30	11 610.53	1.33	11 565.83	1.32
$[FeCl_4]^{2-}$	2	2	4.2	1.00	11 614.73	0.99	11 573.54	0.96	11 611.41	0.99	11 566.72	0.96
$[FeCl_4]^{-}$	3	5/2	77	0.30	11 616.10	0.43	11 574.78	0.43	11 613.09	0.35	11 568.26	0.35
$[FeBr_4]^{-}$	3	5/2	77	0.36	11 616.05	0.45	11 574.74	0.45	11 613.06	0.36	11 568.23	0.36
$[FeCl_6]^{3-}$	3	5/2	78	0.53	11 615.40	0.72	11 574.12	0.71	11 612.38	0.62	11 567.57	0.62
$[Fe(H_2O)_6]^{3+}$	3	5/2	78	0.50	11 615.30	0.75	11 574.02	0.75	11 612.33	0.64	11 567.54	0.64
$[FeF_6]^{3-}$	3	5/2	0	0.69	11 615.91	0.51	11 574.61	0.50	11 612.74	0.48	11 567.94	0.48
$[Fe(CN)_6]^{3-}$	3	1/2	143	−0.15	11 617.35	−0.08	11 575.95	−0.08	11 614.14	−0.05	11 569.23	−0.04
$[FeO_4]^{2-}$	6	1	143	−0.90	11 613.18	−0.82	11 577.72	−0.84	11 616.43	−0.93	11 571.54	−0.97
r						0.971		0.971		0.981		0.980
rms						0.122		0.122		0.097		0.099
α_{rel}						−0.313		−0.331		−0.294		−0.316
c					11 617.15		11 575.77		11 614.01		11 569.13	

slope expected between experimental and theoretical data, while in both sets of optimized geometries, the pure BPW91 functional shows a significantly better slope in the correlation analysis as compared to the hybrid B3LYP functional (Tables 5−7). Observed slopes for the B3LYP approach found in our test systems (1.09−1.19) are appreciably higher as compared to those reported by Oldfield's group for the same exchange correlation functional (1.04−1.12).[42] Closer analysis of theoretical data (Table 5−7) for sandwich and half-sandwich organometallic compounds using all three geometry sets available suggests that calculated (using B3LYP exchange−correlation functional) electric field gradients for ferrocenes, which were not considered in previous works, are ∼1.3 times larger as compared to experimental values, while an excellent agreement was observed between theoretical (BPW91) and experimental quadrupole splittings for the

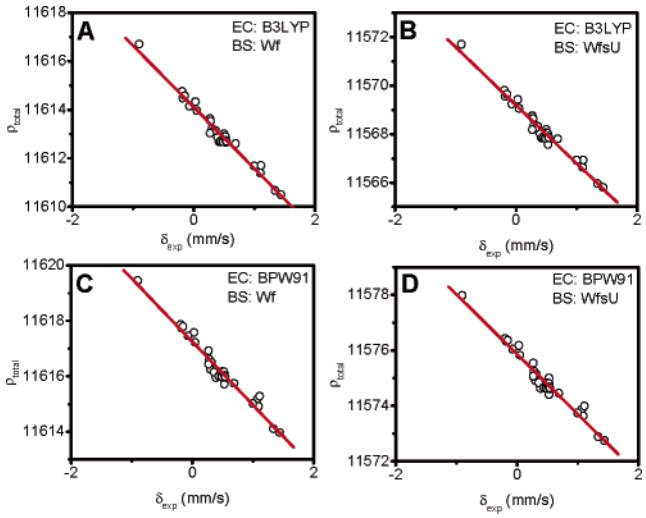

Figure 1. Correlation between experimental isomer shifts (δ_{exp}) and calculated (X-ray geometry test set) total electron density at the ^{57}Fe nucleus (ρ_{total}) using (A) B3LYP functional and Wf basis set; (B) B3LYP functional and WfsU basis set; (C) BPW91 functional and Wf basis set; and (D) BPW91 functional and WfsU basis set.

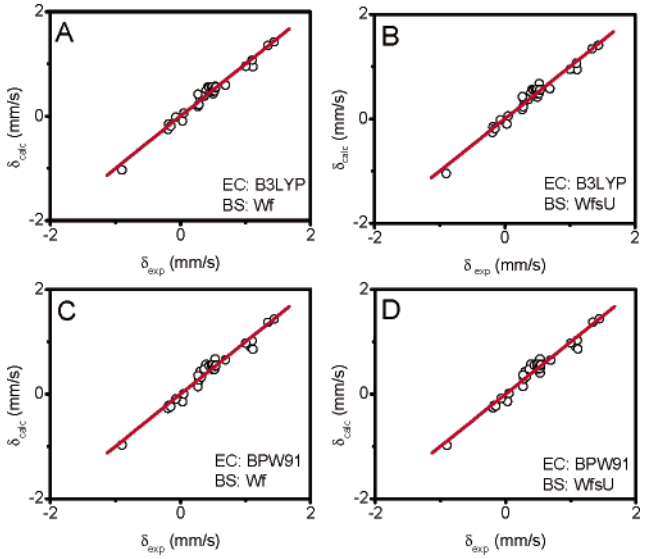

Figure 2. Correlation between experimental (δ_{exp}) and calculated (δ_{calc}) isomer shifts (X-ray geometry test set) using (A) B3LYP functional and Wf basis set; (B) B3LYP functional and WfsU basis set; (C) BPW91 functional and Wf basis set; and (D) BPW91 functional and WfsU basis set.

same complexes. Taking into account that the typical error in calculated quadrupole splittings using a B3LYP exchange−correlation functional for ferrocenes is ∼0.6 mm/s for 12 ferrocenes tested, it is safe to conclude that this exchange−correlation functional should not be recommended for prediction of the complete set of Mössbauer parameters in sandwich organometallic complexes. In the case of half-sandwich organometallic structures, i.e., $CpFe(CO)_2Cl$, $CpFe(CO)_2CH_3$, (cyclobutadiene)$Fe(CO)_3$, and (1,4-butadiene)-$Fe(CO)_3$, performance of the pure BPW91 exchange−correlation functional is also better but the hybrid B3LYP exchange−correlation functional still gives acceptable results. Our results in calculation of quadrupole splittings in ferrocenes are in contrast to the currently generally accepted superiority of hybrid exchange−correlation functionals (i.e., B3LYP) over pure ones (i.e., BPW91) in prediction of Mössbauer spectra parameters in iron-containing complexes. The only principal difference between pure BPW91 and hybrid B3LYP exchange−correlation functionals is the presence of ∼20% Hartree−Fock exchange in the later case.[66,67] To clarify the influence of Hartree−Fock exchange on calculated quadrupole splittings in sandwich organometallic compounds, several ferrocenes have been tested and the results for three ferrocenes are presented in Table 8 and Figure 4.

Results clearly indicate a relationship between the amount of involved Hartree−Fock exchange and calculated quadrupole splitting in ferrocenes, with the observed correlation coefficient of $r > 0.99$ for 14 tested exchange−correlation functionals. Observed dependence can be explained to some extent using well-known second-order perturbation theory.[68] Indeed, unlike the most molecules used for the training sets in DFT calculations of Mössbauer spectra parameters, the principal binding in ferrocenes belongs to the π-type. Accordingly, formation and stability of these compounds heavily depends on the degree of electron d_δ donation from filled d-orbitals of iron to π^* orbitals of the Cp^- ligand, as well as π-back-donation from occupied π-orbitals of the Cp^- ligand to unoccupied d_π orbitals of iron (Supporting Information Figure 7), and such electron density redistribution within a molecule is charge-transfer in nature. According to second-order perturbation theory, the energy of interaction between donor and acceptor orbitals can be expressed as[68]

$$\Delta E = \sum_{i}^{\text{occ}} \sum_{j}^{\text{unocc}} \frac{2(\sum_{\mu} \sum_{\nu} c_{\mu i} c_{\nu j} \beta_{\mu\nu})^2}{|\epsilon_i - \epsilon_j|} \qquad (7)$$

(where ϵ_i and ϵ_j are the molecular orbital energy eigenvalues pertaining to the respective fragments, $c_{\mu i}$ and $c_{\nu j}$ are the coefficients of atomic orbitals φ_μ in molecular orbital i on fragment A and φ_ν in molecular orbital j on fragment B, respectively, and $\beta_{\mu\nu}$ is the resonance integral between φ_μ and φ_ν) and thus depends on the accuracy of calculated energy difference between occupied (donor) and unoccupied (acceptor) orbitals. For sake of simplicity, only two such charge-transfer pairs in ferrocene will be considered (i) charge-transfer from the highest energy (HOMO-3 and HOMO-4) doubly degenerated occupied Cp^- π-orbital to doubly degenerated d_{xz}, d_{yz} (LUMO and LUMO+1) pair, and (ii) charge-transfer from doubly degenerated iron d_{xy}, $d_{x^2-y^2}$ (HOMO and HOMO-1) orbitals to doubly degenerated Cp^- π^*-orbitals (Supporting Information Figure 7). Indeed, the calculated (using pure DFT methods) energy differences for these two pairs of orbitals (∼4.6 and ∼5 eV, respectively) are very close to the first two observed charge-transfer bands in ferrocene (4.67 eV, band IV; 5.17 eV, band V).[69] When

(66) Foresman, J. B.; Frisch, Aeleen. *Exploring Chemistry with Electronic Structure Methods*: 2nd ed.; Gaussian, Inc.: Pittsburgh, 1996.
(67) Parr, R. G.; Yang, W. *Density-Functional Theory of Atoms and Molecules*; Oxford University Press: Oxford, 1989.
(68) Klopman, G. *J. Am. Chem. Soc.* **1968**, *90*, 223−234.
(69) Sohn, Y. S.; Hendrickson, D. N.; Gray, H. B. *J. Am. Chem. Soc.* **1971**, *93*, 3603−3612.

Table 5. Experimental and Calculated ^{57}Fe Mössbauer Quadrapole Splittings for the X-ray Geometry Test Set

			experimental		calculated			
					BPW91/Wf	BPW91/WfsU	B3LYP/Wf	B3LYP/WfsU
compound	OS	S	T (K)	ΔE_Q (mm/s)	ΔE_Q (mm/s)	ΔE_Q (mm/s)	ΔE_Q (mm/s)	ΔE_Q (mm/s)
$Fe(CO)_5$	0	0	4.2	+2.52[a]	2.24	2.24	2.55	2.55
$(butadiene)Fe(CO)_3$	0	0	77	−1.46[b]	−1.45	−1.45	−1.58	−1.58
$CpFe(CO)_2Cl$	2	0	4.2	1.82[a]	1.68	1.68	1.96	1.96
$CpFe(CO)_3$	2	0	78	1.88[b]	1.94	1.94	2.16	2.16
Fc D_{5h}	2	0	80	+2.40[c]	2.34	2.34	3.10	3.13
Fc D_{5d}	2	0	80	+2.40[c]	2.39	2.39	3.08	3.09
FcCN	2	0	80	2.36[b]	2.28	2.29	3.06	3.06
$FcCN_3Vy$	2	0	RT	2.05[d]	2.15	2.15	2.95	2.95
FcC≡CH	2	0	80	2.23[e]	2.22	2.23	3.03	3.03
Fc(COMe)	2	0	80	2.27[f]	2.17	2.18	2.98	2.99
$Fc(COMe)_2$	2	0	80	2.27[f]	2.08	2.09	2.94	2.94
$Fc(CO_2Me)$	2	0	80	2.30[f]	2.27	2.27	3.05	3.05
$Fc(CO_2Me)_2$	2	0	80	2.34[f]	2.20	2.20	3.03	3.04
$Fc(CO_2H)$	2	0	RT	2.16[f]	2.23	2.23	3.00	3.00
$Fc(CO_2H)_2$	2	0	80	2.16[f]	2.14	2.14	2.94	2.94
$PcFePy_2$	2	0	4.2	+1.96[g]	2.18	2.18	1.78	1.77
$PcFe(mepip)_2$	2	0	RT	2.28[g]	2.49	2.49	2.09	2.09
$[Fe(CN)_5NO]^{2-}$	2	0	77	1.72[h]	1.93	1.93	2.17	2.17
$Fe(phen)_2Cl_2$	2	2	77	(−)3.27[i]	−1.97	−1.97	−3.08	−3.08
$Fe(bipy)_2Cl_2$	2	2	78	(−)3.40[h]	−2.19	−2.19	−3.22	−3.22
$FePy_4Cl_2$	2	2	4.2	3.14[h]	2.74	2.74	3.33	3.33
$[Fe(H_2O)_6]^{2+}$	2	2	200	+3.40[h]	3.16	3.16	3.28	3.28
$[FeCl_4]^{2-}$	2	2	4.2	−3.27[h]	−3.51	−3.67	−3.63	−3.76
$[Fc]^+$	3	1/2	78	0.00[f]	−0.29	−0.28	0.20	0.20
PcFeCl	3	5/2	77	2.56[g]	2.33	2.33	2.47	2.46
$[Fe(bipy)_2Cl_2]^+$	3	5/2	RT	−0.24[i]	−0.42	−0.42	−0.47	−0.47
$[Fe(phen)_2Cl_2]^+$	3	5/2	80	0.05[b]	0.44	0.44	0.49	0.49
$[FeCl_4]^-$	3	5/2	77	0.00[h]	0.00	0.00	0.00	0.00
$[FeBr_4]^-$	3	5/2	77	0.00[h]	0.00	0.00	0.00	0.00
$[FeCl_6]^{3-}$	3	5/2	78	0.00[i]	0.00	0.00	0.00	0.00
$[Fe(H_2O)_6]^{3+}$	3	5/2	78	0.00[j]	0.00	0.00	0.00	0.00
r					0.985	0.983	0.986	0.985
rms					0.301	0.317	0.355	0.361
slope					0.885	0.892	1.089	1.095

[a] Reference 64. [b] Reference 57. [c] Reference 45. [d] This work, see Supporting Information for details. [e] Reference 76. [f] Reference78. [g] Reference 77. [h] Reference 58. [i] Reference 75. [j] Reference 79.

Table 6. Experimental and Calculated ^{57}Fe Mössbauer Quadrapole Splittings for the B3LYP Geometry Test Set

			experimental		calculated			
					BPW91/Wf	BPW91/WfsU	B3LYP/Wf	B3LYP/WfsU
structure	OS	S	T (K)	ΔE_Q (mm/s)	ΔE_Q (mm/s)	ΔE_Q (mm/s)	ΔE_Q (mm/s)	ΔE_Q (mm/s)
$[Fe(CO)_4]^{2-}$	−2	0	RT	0.00[a]	0.00	0.00	0.00	0.00
$Fe(CO)_5$	0	0	4.2	+2.52	2.37	2.37	2.71	2.71
$(cyclobutadiene)Fe(CO)_3$	0	0	78	+1.52[b]	1.54	1.54	1.64	1.64
$(butadiene)Fe(CO)_3$	0	0	77	−1.46	−1.44	−1.44	−1.56	−1.57
$CpFe(CO)_2Me$	2	0	78	1.76[b]	1.86	1.86	2.17	2.17
$CpFe(CO)_2Cl$	2	0	4.2	+1.82	1.76	1.76	2.02	2.02
Fc D_{5h}	2	0	80	+2.40	2.61	2.62	3.43	3.43
Fc D_{5d}	2	0	80	+2.40	2.67	2.67	3.48	3.49
FcCN	2	0	80	2.36	2.49	2.50	3.33	3.33
$FcCN_3Vy$	2	0	RT	2.05	2.30	2.30	3.20	3.20
$[Fe(CN)_5NO]^{2-}$	2	0	77	1.72	1.74	1.74	1.96	1.96
$[Fe(H_2O)_6]^{2+}$	2	2	200	+3.40	3.66	3.66	3.80	3.80
$[FeCl_4]^{2-}$	2	2	4.2	−3.27	−3.56	−3.35	−3.57	−3.57
$[FeCl_4]^-$	3	5/2	77	0.00	0.00	0.00	0.00	0.00
$[FeBr_4]^-$	3	5/2	77	0.00	0.00	0.00	0.00	0.00
$[FeCl_6]^{3-}$	3	5/2	78	0.00	0.00	0.00	0.00	0.00
$[Fe(H_2O)_6]^{3+}$	3	5/2	78	0.00	0.00	0.00	0.00	0.00
r					0.998	0.998	0.988	0.988
rms					0.108	0.108	0.333	0.334
slope					1.041	1.041	1.193	1.193

[a] Reference 74. [b] Reference 58.

calculated energy differences between first and second pairs of orbitals were plotted against percentage of Hartree−Fock exchange involved in the calculations and calculated quadrupole splittings (Figure 5), correlations with $r > 0.99$ have been observed. Such strong correlations are clearly indicative of the importance of accurate prediction of not only energy

Table 7. Experimental and Calculated ^{57}Fe Mössbauer Quadrapole Splittings for the BP86 Geometry Test Set

			experimental		calculated			
					BPW91/Wf	BPW91/WfsU	B3LYP/Wf	B3LYP WfsU
structure	OS	S	T (K)	ΔE_Q (mm/s)	ΔE_Q (mm/s)	ΔE_Q (mm/s)	ΔE_Q (mm/s)	ΔE_Q (mm/s)
$[Fe(CO)_4]^{2-}$	−2	0	RT	0.00	0.00	0.00	0.00	0.00
$Fe(CO)_5$	0	0	4.2	+2.52	2.19	2.19	2.52	2.52
(cyclobutadiene)$Fe(CO)_3$	0	0	78	+1.52	1.52	1.52	1.62	1.62
(butadiene)$Fe(CO)_3$	0	0	77	−1.46	−1.36	−1.36	−1.48	−1.48
$CpFe(CO)_2Me$	2	0	78	1.76	1.75	1.75	2.05	2.06
$CpFe(CO)_2Cl$	2	0	4.2	+1.82	1.66	1.66	1.92	1.92
Fc D_{5h}	2	0	80	+2.40	2.33	2.33	3.12	3.12
Fc D_{5d}	2	0	80	+2.40	2.39	2.39	3.17	3.18
FcCN	2	0	80	2.36	2.20	2.21	3.01	3.01
$FcCN_3Vy$	2	0	RT	2.05	2.03	2.03	2.88	2.88
$[Fe(CN)_5NO]^{2-}$	2	0	77	1.72	1.92	1.92	2.17	2.17
$[Fe(H_2O)_6]^{2+}$	2	2	200	+3.40	3.67	3.66	3.81	3.81
$[FeCl_4]^{2-}$	2	2	4.2	−3.27	−3.62	−3.61	−3.86	−3.86
$[FeCl_4]^{-}$	3	5/2	77	0.00	0.00	0.00	0.00	0.00
$[FeBr_4]^{-}$	3	5/2	77	0.00	0.00	0.00	0.00	0.00
$[FeCl_6]^{3-}$	3	5/2	78	0.00	0.00	0.00	0.00	0.00
$[Fe(H_2O)_6]^{3+}$	3	5/2	78	0.00	0.00	0.00	0.00	0.00
r					0.996	0.996	0.993	0.993
rms					0.155	0.155	0.238	0.238
slope					1.022	1.022	1.174	1.174

differences within occupied and unoccupied orbital subsets but also computed HOMO−LUMO (or strictly speaking occupied-unoccupied orbitals) energy gap accuracy, which strongly depends on the amount of Hartree−Fock exchange involved in the calculations.

It is well known that pure exchange−correlation functionals give a closer to experiment HOMO−LUMO energy gap as compared to the hybrid functionals.[67] For instance, the early success of Slater's empircal electron excitation method for prediction of vertical excitation energies[70,71] along with the ligand-field-based method for prediction of EPR parameters in transition metal complexes[71,72] reflects a relatively accurate prediction of the HOMO−LUMO energy gap using X_α and other pure DFT approaches. An observed fact that calculated quadrupole splittings in other tested ferrocenes

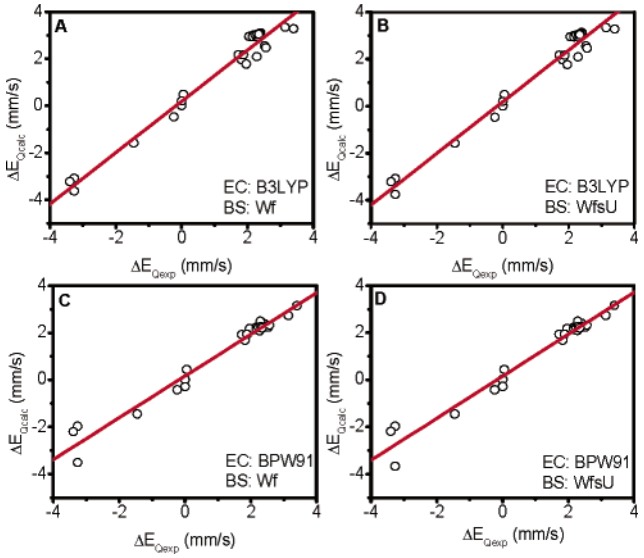

Figure 3. Correlation between experimental (ΔE_{Qexp}) and calculated (ΔE_{Qcalc}) quadrupole splittings (X-ray geometry test set) using (A) B3LYP functional and Wf basis set; (B) B3LYP functional and WfsU basis set; (C) BPW91 functional and Wf basis set; and (D) BPW91 functional and WfsU basis set.

Table 8. Calculated Electric Field Gradient Component, V_{zz}, and Quadrupole Splitting (ΔE_Q, mm/s) Values for Ferrocene (D_{5h}), FcCN, and $FcCN_3Vy$ (X-ray geometries) vs Percentage of Hartree−Fock Exchange Involved in the DFT Functional

		Fc D_{5h}		FcCN		$FcCN_3Vy$	
functional	HF %	V_{zz}	ΔE_Q	V_{zz}	ΔE_Q	V_{zz}	ΔE_Q
Xα	0	−1.427	2.31	−1.401	2.27	−1.281	2.14
LSDA	0	−1.417	2.30	−1.393	2.26	−1.272	2.13
BP86	0	−1.447	2.34	−1.413	2.29	−1.289	2.15
BPW91	0	−1.442	2.34	−1.408	2.28	−1.283	2.14
BLYP	0	−1.486	2.41	−1.448	2.35	−1.323	2.20
VSXC	0	−1.539	2.49	−1.495	2.42	−1.363	2.25
B3P86	20	−1.892	3.07	−1.851	3.00	−1.762	2.89
B3PW91	20	−1.889	3.06	−1.846	2.99	−1.757	2.88
B3LYP	20	−1.934	3.13	−1.889	3.06	−1.803	2.95
B98	21.98	−1.979	3.21	−1.937	3.14	−1.853	3.03
PBE1PBE	25	−1.978	3.20	−1.931	3.13	−1.853	3.03
BH and H	50	−2.545	4.12	−2.483	4.02	−2.446	3.98
BH and HLYP	50	−2.615	4.24	−2.543	4.12	−2.509	4.08
HF	100	−3.370	5.46	−3.258	5.28	−3.247	5.27
exptl			2.40		2.36		2.05

correlate (r > 0.99) with HOMO−LUMO energy gap supports our hypothesis (Supporting Information Figure 8).

(70) Balagopalakrishna, C.; Dimbrough, J. T.; Westmorland, T. D. *Inorg. Chem.* **1996**, *35*, 7758−7768. Sunil, K. K.; Harrison, J. F.; Rogers, Max T. *J. Chem. Phys.* **1982**, *76*, 3087−3097. Waller, W. G.; Rogers, Max T. *J. Magn. Reson.* **1975**, *18*, 39−56.
(71) Swann, J.; Westmoreland, T. D. *Inorg. Chem.* **1997**, *36*, 5348−5357.
(72) Wilson, G. L.; Greenwood, R. J.; Pilbrow, J. R.; Spence, J. T.; Wedd, A. G. *J. Am. Chem. Soc.* **1991**, *113*, 6803−6812. Sunil, K. K.; Rogers, M. T. *Inorg. Chem.* **1981**, *20*, 3283−3287. Sunil, K. K.; Harrison, J. F.; Rogers, M. T. *J. Chem. Phys.* **1982**, *76*, 3078−3086.
(73) Kerler, W.; Neuwirth, W.; Fluck, E. *Z. Phys.* **1963**, *175*, 200.
(74) Havlin, R. H.; Godbout, N.; Salzmann R.; Wojdelski, M.; Arnold, W.; Shultz, C. E.; Oldfield, E. *J. Am. Chem. Soc.* **1998**, *120*, 3144−3151.
(75) Schmidt, G.; Barbenheim, G.; Boese, R. *Z. Naturforsch. B.* **1985**, *40*, 787.
(76) Schottenberger, H.; Buchmeiser, M. R.; Herber, R. H. *J. Organomet. Chem.* **2000**, *612*, 1−8.
(77) Hanack, M.; Keppeler, U.; Lange, A.; Hirsch, A.; Dieing, R. In *Phthalocyanines: Properties and Applications*; Lever, A. B. P., Leznoff, C. C., Eds.; Wiley-VCH: New York, 1993; Vol. 2, pp 43−96.
(78) Stukan, P. A.; Gubin, S. P.; Nesmeyakov, A. N.; Goldanskii, V. I. Makarov, E. F. *Theor. Exp. Chem.* **1966**, *2*, 805−811.

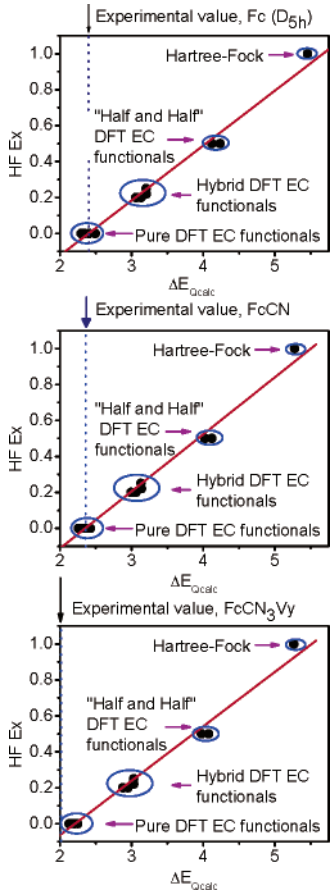

Figure 4. Correlation between applied exchange−correlation functionals and calculated quadrupole splittings in ferrocene (top), cyanoferrocene (middle), and tricyanovinylferrocene (bottom).

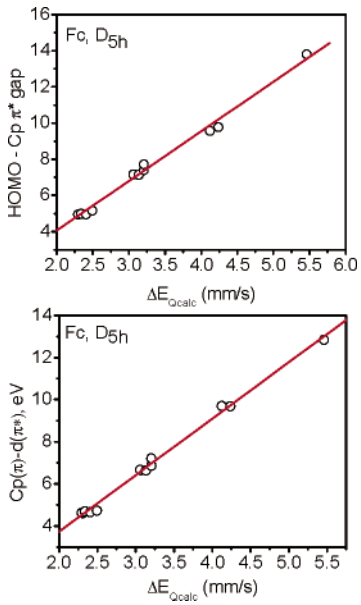

Figure 5. Correlation between calculated quadrupole splittings and energy gap between Fe (d_{xy}, $d_{x^2-y^2}$) and Cp(π*) (top) and Cp(π) and Fe (d_{xz}, d_{yz}) (bottom) orbitals.

Conclusions

In the present work, three sets of molecular geometries, pure, as well as hybrid, DFT exchange−correlation functionals and two basis sets for the iron nuclei have been tested in the calculation of Mössbauer isomer shifts and quadrupole splittings. The good-quality linear correlation between experimental isomer shifts and calculated electronic densities at Mössbauer nuclei has been observed for all training sets of molecules, which cover a wide range of ligand types, as well as oxidation and spin states. It has been found that, for Wachter's full-electron basis set applied at the iron nuclei, uncontraction of the s-part of the basis set does not lead to an appreciable improvement of calculated isomer shifts, and thus, a traditional contraction scheme can be used with a high level of confidence, which allows one to calculate Mössbauer spectra parameters several times faster as compared to the uncontracted basis set approach. The observed correlation coefficients for all three sets of geometries (X-ray, B3LYP, and BP86 optimized) are close to one another and predominantly depend on the employed exchange−correlation functional with the hybrid B3LYP functional being slightly better as compared with the pure BPW91 functional. Both exchange−correlation functionals can be used for the calculation of Mössbauer isomer shifts in organometallic compounds including ferrocenes. Despite excellent correlations between experimental and calculated quadrupole splittings in all three training sets, it has been found that hybrid B3LYP exchange−correlation functional completely fails to predict accurate quadrupole splittings in ferrocenes, while performance of the pure BPW91 functional for the same systems was excellent. It has been found that adequate prediction of Mössbauer quadrupole splittings in ferrocene-like complexes require accurate calculation of the HOMO−LUMO energy gap, which can probably be achieved only by employing one of the pure DFT exchange−correlation functionals.

Overall, previously demonstrated for biological systems, phthalocyanines, porphyrins, and other Fe^{II} and Fe^{III} complexes, high potential of the modern DFT approach for prediction of Mössbauer isomer shifts and quadrupole splittings in ^{57}Fe-containing systems has been confirmed for all model systems used in this work, while some recommendations were made for accurate calculations of the electric field gradients in ferrocenes and other organometallic sandwich compounds.

Acknowledgment. We thank Research Corporation (grant CC6766) and University of Minnesota (Grant-in-Aid to V.N.N.) for financial support and Minnesota Supercomputing Institute for the generous support of computer time. We also acknowledge Professor Eric Oldfield and Dr. Douglas Fox for the numerous discussions and interest.

(79) Earls, D. E.; Axtmann, R. C.; Leftkowitz, Y. H. I. *J. Phys. Chem. Sol.* **1968**, *29*, 1859−1863.

(80) We used the −0.18 mm/s value for isomer shift in $Fe(CO)_5$ compound in order to compare our results with those published by Oldfield et al. (*J. Am. Chem. Soc.* **2002**, *124*, 7829, ref 44). The values available in the literature vary from 0.00 to −0.18 mm/s. The use of the 0.00 mm/s value for the isomer shift in iron pentacarbonyl does not change appreciably both correlation coefficients and α_{rel} (Supporting Information Table 1).

Supporting Information Available: Correlations between calculated total electron densities and experimental isomer shifts for B3LYP and BP86 optimized geometries, correlations between experimental and calculated isomer shifts and quadrupole splittings for B3LYP and BP86 optimized geometries, bonding diagram for ferrocene, correlation between HOMO−LUMO energy gap and calculated quadrupole splittings in ferrocenes. This material is available free of charge via the Internet at http://pubs.acs.org.

IC061176Q